ACS APPLIED MATERIALS & INTERFACES

Research Article

www.acsami.org

Conductive Water/Alcohol-Soluble Neutral Fullerene Derivative as an Interfacial Layer for Inverted Polymer Solar Cells with High Efficiency

Chao Yi,[†] Kan Yue,[†] Wen-Bin Zhang,[†] Xiaocun Lu,[†] Jianhui Hou,[‡] Yongfang Li,[‡] Lin Huang,[§] George R. Newkome,[†] Stephen Z. D. Cheng,[†] and Xiong Gong*[,†]

[†]College of Polymer Science and Polymer Engineering, The University of Akron, Akron, Ohio 44325, United States

[‡]Institute of Chemistry, Chinese Academy of Science, Beijing, 100190, People's Republic of China

[§]Nano Surfaces Division, Bruker Corporation, 112 Robin Hill Road, Santa Barbara, California 93117, United States

Supporting Information

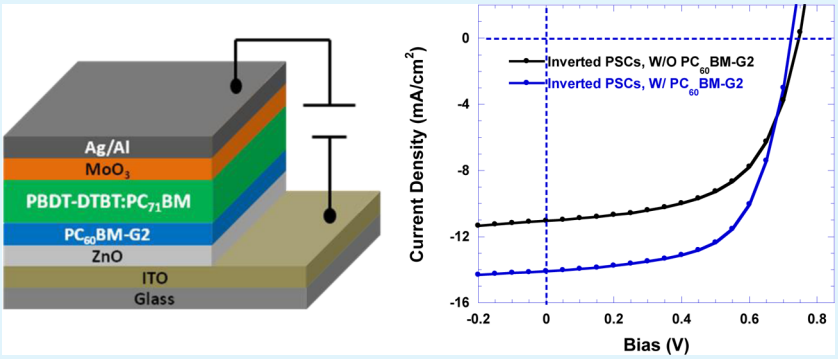

ABSTRACT: Dipole induced vacuum level shift has been demonstrated to be responsible for the enhanced efficiency in polymer solar cells (PSCs).The modified energy level alignment could reduce the energy barrier and facilitate charge transport, thereby increasing the efficiency of PSCs. Herein, we report a new mechanism toward enhanced efficiency by using a nondipolar water/alcohol-soluble neutral fullerene derivative to reengineer the surface of the zinc oxide (ZnO) electron extraction layer (EEL) in inverted PSCs. Because of the neutral property (ion-free) of the fullerene derivatives, no dipole moment was introduced at the EEL/active layer interface. A negligible change in open-circuit voltage was observed from inverted PSCs with the neutral fullerene derivative layer. The neutral fullerene derivative layer greatly increased the surface electronic conductivity of the ZnO EEL, suppressed surface charge recombination, and increased the short-circuit current density and fill factor. An overall power conversion efficiency increase of more than 30% from inverted PSCs was obtained. These results demonstrate that the surface electronic conductivity of the EEL plays an important role in high performance inverted PSCs.

KEYWORDS: *inverted polymer solar cells, electron extraction layer, neutral, surface electronic conductivity, power conversion efficiency*

INTRODUCTION

Polymer solar cells (PSCs), based on the bulk heterojunction (BHJ) composite of conjugated polymers blended with fullerene derivatives, have been attracting great attention in both academic and industrial sectors for the promising future as one of the renewable energy sources.[1] BHJ PSCs are characterized by their light weight, high flexibility, and low cost in large-scale commercialization.[2,3] In order to enhance the power conversion efficiency (PCE) of PSCs, conjugated polyelectrolytes and/or ionic C_{60} derivatives have been used as an interfacial layer to modify the band alignment between the BHJ active layer and the electrodes.[4−6] The dipole formed by the counterions from either conjugated polyelectrolytes or ionic C_{60} derivatives has been demonstrated to contribute to the minimization of the energy barrier for electron extraction from the BHJ active layer toward the cathode. This resulted in enhanced PCE of PSCs incorporated with either conjugated polyelectrolytes or ionic C_{60} derivatives.[7−10] The studies by ultraviolet photoemission spectroscopy and/or Kelvin probe microscopy indicated that enlarged, open-circuit voltage (V_{OC}) was attributed to the presence of a dipole moment, which effectively shifts the vacuum level on the surface of the metal electrode, thus reducing the effective work function of the metal electrode.[11,12] Recently, Heeger's group reported the enhanced efficiency of PSCs by using the polar solvent methanol (MeOH) to treat the surface of the BHJ active layer. The report further revealed that the enhanced device performance was attributed to the increased surface charge density, which originated from an enlarged built-in voltage across PSCs.[13] However, the origins of the enhanced, short-circuit current (J_{SC}) and fill factor (FF) are still not clear and are difficult to be

Received: June 3, 2014
Accepted: July 28, 2014
Published: July 28, 2014

Scheme 1. Synthetic Route of $PC_{60}BM$-G2

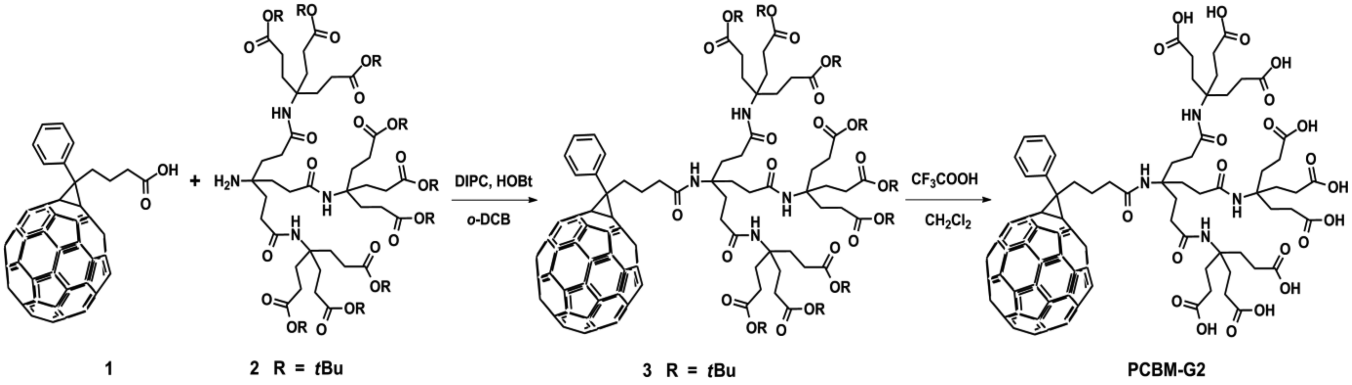

attributed simply to a modified energy level alignment by the dipole moment.[13,14]

Recently, our group demonstrated that reengineering the surface of the zinc oxide (ZnO) electron extraction layer (EEL) from the inverted PSCs with conjugated polyelectrolytes gave a ca. 38% enhancement in PCEs. It was determined that the surface electronic conductivity of the ZnO EEL plays an important role in enhanced J_{SC} and FF.[15] In order to further study the origins of both enhanced J_{SC} and FF, herein, we report a study of using a conductive novel water/alcohol-soluble neutral fullerene derivative ($PC_{60}BM$-G2; see the Experimental Section) as an interfacial layer for the inverted PSCs. We found that over 30% enhancement in PCEs was observed from the inverted PSCs with the $PC_{60}BM$-G2 layer to modify the surface of the ZnO EEL compared to those without the $PC_{60}BM$-G2 layer.

EXPERIMENTAL SECTION

Synthesis and Characterization of $PC_{60}BM$-G2. [6,6]-Phenyl-C_{61}-butyric acid (135 mg, 150 μmol), compound **2** (Scheme 1) (238 mg, 165 μmol), and hydroxybenzotriazole (HOBt, 22 mg, 165 μmol) were added into a round-bottom flask (50 mL) equipped with a magnetic stir bar, and then freshly dried *o*-dichlorobenzene (*o*-DCB, 10 mL) was input into the above flask to dissolve all of the solids. The flask was capped by a rubber septum and cooled to 0 °C. After that, *N*,*N*′-diisopropylcarbodiimide (DIPC, 62 mg, 495 μmol) was added. The mixture was warmed to 25 °C and stirred for 24 h. The white precipitate was then filtered, and the filtrate was washed with water and brine, dried over Na_2SO_4, and evaporated in vacuo. The residue was purified by flash column chromatography on silica gel with toluene/EtOAc (v/v = 4/1) as the eluent to afford (75%) the product **3** (Scheme 1), as a brown powder: 260 mg. Compound **3** (120 mg, 52 μmol) was dissolved in a mixture of trifluoroacetic acid (2 mL) and CH_2Cl_2 (4 mL). The resulting solution was stirred at 25 °C for 12 h. The solvent was then removed in vacuo, and the residue solid was washed with $CHCl_3$ (10 mL) and dried in vacuo to afford (95%) the product as a brown powder: 89 mg.

Absorption Spectrum of $PC_{60}BM$-G2. The absorption spectrum of $PC_{60}BM$-G2 thin film was measured by a HP 8453 UV−vis spectrophotometer.

Cyclic Voltammetry Measurement. The electrochemical cyclic voltammetry (CV) was operated with a three-electrode system (Pt disk as working electrode, Pt wire as counter electrode, and Ag/AgCl as reference electrode). The electrolyte is 0.1 mol L^{-1} tetrabutylammoniumhexafluorophosphate (Bu_4NPF_6) in MeCN. Ferrocence/ferrocenium (Fc/Fc^+) was used for calibration.

AFM Measurement. AFM images were taken on a Nano-Scope NS3A system (Digital Instrument) to investigate the surface topology of ZnO, $PC_{60}BM$-G2/ZnO, and PBDT-DTBT:$PC_{71}BM$ BHJ composites on pristine ZnO and on $PC_{60}BM$-G2/ZnO precoated ITO substrates. Peak force tunneling AFM (PFTUNA) was used to investigate the surface electronic conductivity of ZnO and $PC_{60}BM$-G2/ZnO thin layers. An AFM tip coated with 20 nm Pt/Ir on both the front and back sides was put into contact with the surfaces of ZnO and $PC_{60}BM$-G2/ZnO thin films. The PFTUNA module was used to measure TUNA current with bias voltage applied to ZnO and $PC_{60}BM$-G2/ZnO thin films.

Device Fabrication and Characterization. Two inverted PSCs, one with a structure of ITO/ZnO/PBDT-DTBT:$PC_{71}BM$/MoO_3/Ag and the other with a structure of ITO/ZnO/$PC_{60}BM$-G2/PBDT-DTBT:$PC_{71}BM$/MoO_3/Ag, and a normal PSC with a structure of ITO/PEDOT:PSS/PBDT-DTBT:$PC_{71}BM$/Al were fabricated. A ZnO thin film with a thickness of ∼40 nm was made by spin-coating the precursor solution on the ITO-glass substrate with 3000 rpm for 10 s, followed by annealing at 200 °C for 1 h. The ZnO thin film was ultrasonicated in isopropanol and was then stored in the oven overnight for further device fabrication. For the inverted PSCs with a device structure of ITO/ZnO/$PC_{60}BM$-G2/PBDT-DTBT:$PC_{71}BM$/MoO_3/Ag, a thickness ∼ 5 nm (measured by tapping mode AFM) of $PC_{60}BM$-G2 was spin-coated on top of the ZnO thin film from 0.3 mg/mL methanol solution with 3000 rpm for 20 s. The PBDT-DTBT:$PC_{71}BM$ (1:2 by weight) thin film with a thickness of 70 nm was spin-coated on top of either the ZnO thin film or the $PC_{60}BM$-G2/ZnO thin film from *o*-dichlorobenzene solution. Next, MoO_3 with a thickness of 10 nm was thermally evaporated on top of the PBDT-DTBT:$PC_{71}BM$ BHJ composite layer, as the hole extraction layer. Then, a silver top was thermally evaporated through a shadow mask with an area of 0.045 cm^2 as the top electrode. For the normal device, precleaned ITO substrates were put in UV-ozone for 40 min. Then, ∼30 nm PEDOT:PSS was spin-cast from aqueous solution. The active layer was fabricated the same as that in the inverted device fabrication. Finally, a 100 nm aluminum electrode was thermally deposited through the same shadow mask. The devices were characterized by using a Newport Air Mass 1.5 Global (AM 1.5G) full spectrum solar simulator with an irradiation of 100 mW m^{-2} calibrated by standard silicon solar cells. The current density−voltage (J−V) characteristics were measured using a Keithley 2400 source meter. The polymer material PBDT-DTBT was provided by Dr. Jianhui Hou and Yongfang Li from the Institute of Chemistry, Chinese Academy of Science. The $PC_{71}BM$ was bought from Solenne BV, The Netherlands, and used without further purification. MoO_3 99.5% was bought from Alfa Aesar. The *o*-dichlorobenzene (99%) and methanol (99.8%) were purchased from Sigma-Aldrich and were used without further purification. The PEDOT:PSS (Clevios HTL Solar) was purchased from Heraeus and used as received.

RESULTS AND DISCUSSION

Scheme 1 presents the synthetic route for $PC_{60}BM$-G2, which was synthesized in two steps. Promoted by *N*,*N*′-diisopropylcarbodiimide (DIPC) and hydroxybenzotriazole (HOBt), the reaction between [6,6]-phenyl-C_{61}-butyric acid (**1**) and a reported amine dendron[16,17] (**2**) afforded **3**, which was further

deprotected in a mixture of trifluoroacetic acid and methylene chloride to release the carboxylic acid groups. After deprotection, the existence of nine carboxylic acid groups in $PC_{60}BM$-G2 instilled good solubility in highly polar solvents such as alcohol, MeOH, and dimethyl sulfoxide (DMSO). The details for the synthesis and characterization of $PC_{60}BM$-G2 are provided in the Supporting Information.

The UV−visible absorption spectrum of $PC_{60}BM$-G2 thin film is shown in Figure 1. The $PC_{60}BM$-G2 thin film shows a strong absorption ranging from 200 to 350 nm with a negligible absorption from 400 to 900 nm. This feature indicates that a thin film of $PC_{60}BM$-G2 can act as an interfacial layer on top of the ZnO EEL,[18] which allows visible light to pass into the BHJ active layer. Both the lowest unoccupied molecular orbital (LUMO) and the highest occupied molecular orbital (HOMO) energy levels of $PC_{60}BM$-G2 were estimated based on the electrochemical data observed from cyclic voltammetry (CV) measurement.[19] From the oxidation and reduction peaks (Figure S5, Supporting Information), the LUMO and HOMO energy levels of $PC_{60}BM$-G2 are estimated to be −3.72 and −5.76 eV, respectively. These values are similar to those from [6,6]-phenyl-C_{71}-butyric acid ($PC_{71}BM$),[20] indicating that there is matched band alignment between $PC_{60}BM$-G2 and $PC_{71}BM$ and there is a negligible energy barrier for separated electrons being extracted from the BHJ composite by the thin layer of $PC_{60}BM$-G2 to the respective electrode (Scheme 2).[21] Therefore, the V_{OC} from the inverted PSCs incorporating the $PC_{60}BM$-G2 interfacial layer is expected to be the same as those without the $PC_{60}BM$-G2 interfacial layer.[6,10]

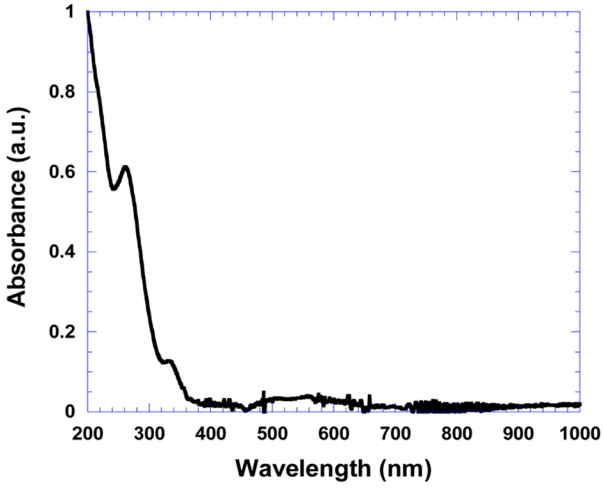

Figure 1. Absorption spectrum of $PC_{60}BM$-G2 thin film.

The inverted devices were fabricated to investigate the photovoltaic properties of PSCs with and without the $PC_{60}BM$-G2 interfacial layer. A conventional device with a structure of ITO/PEDOT:PSS/BHJ composite/Al was also fabricated for comparison studies. Here, ITO is indium tin oxide and PEDOT:PSS is poly(3,4-ethylenedioxythiophene):poly(styrenesulfonate), respectively. The active layer consists of poly[4-(4-(2-ethylhexyl)-5-(8-((2-ethylhexyl)oxy)-4-((2-ethyloctyl)oxy)benzo[1,2-*b*:4,5-*b*′]dithiophen-2-yl)thiophen-2-yl)-*alt*-7-(4-(2-ethylhexyl)thiophen-2-yl)benzo[*c*][1,2,5]thiadiazole] (PBDT-DTBT)[22] and $PC_{71}BM$. The device structures of the inverted PSCs, band alignments among the materials used for construction of the inverted PSCs, and molecular structures

Scheme 2. (a) Device Architecture for the Inverted Polymer Solar Cells. (b) Molecular Structures of PBDT-DTBT and $PC_{71}BM$. (c) LUMO and HOMO Energy Levels of PBDT-DTBT, $PC_{71}BM$, MoO_3, ZnO and Work Functions of ITO and Ag

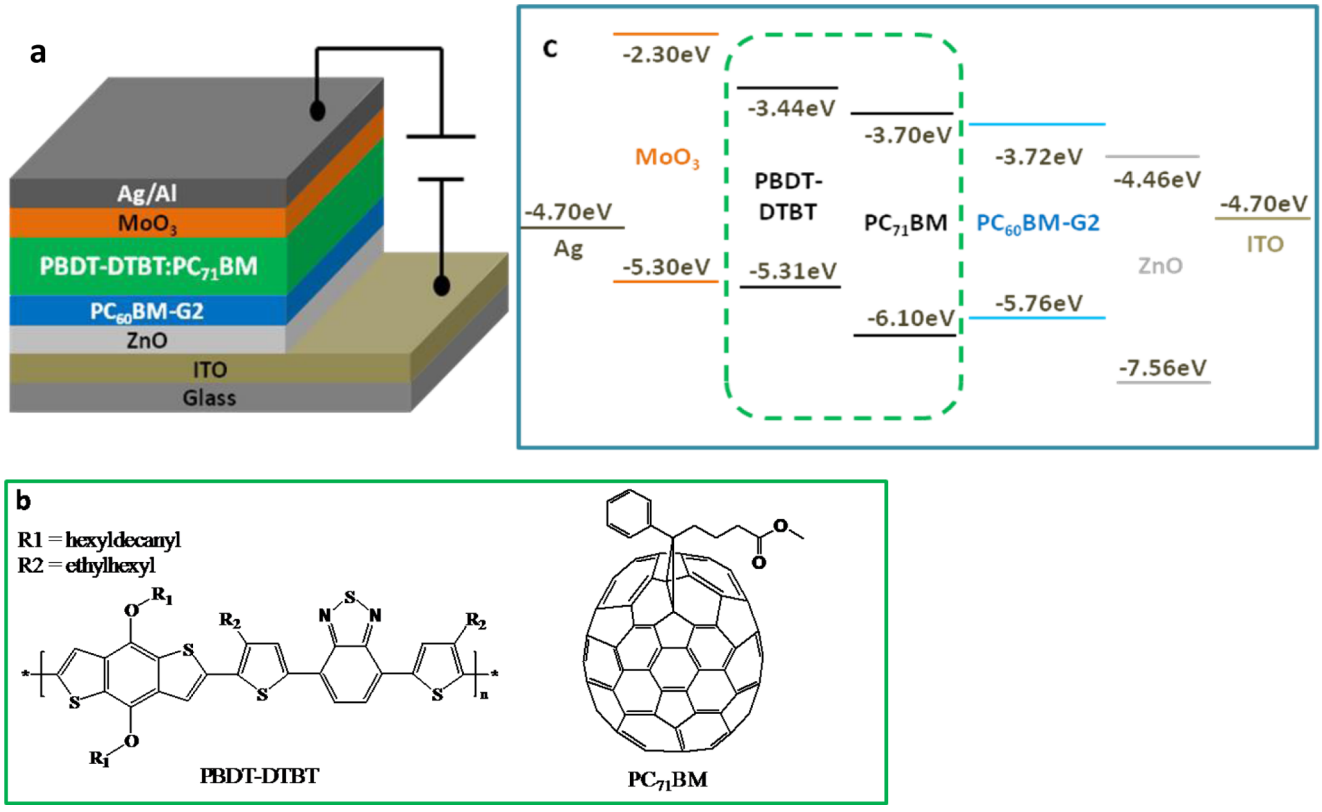

of PBDT-DTBT and $PC_{71}BM$ are shown in Scheme 2. Figure 2 shows $J-V$ characteristics of the conventional PSCs and the

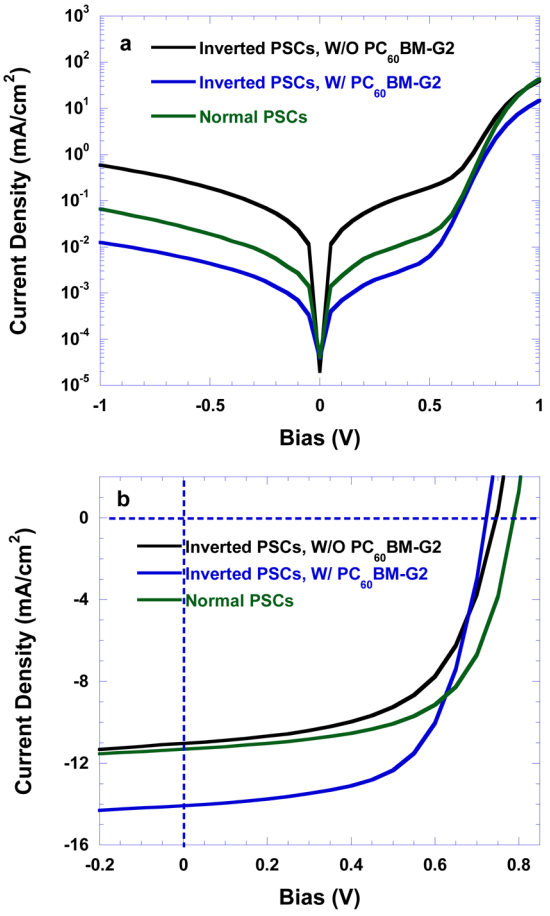

Figure 2. $J-V$ characteristics of the conventional PSCs (normal PSCs, ITO/PEDOT:PSS/PBDT-DTBT:$PC_{71}BM$/MoO_3/Ag), the inverted PSCs with $PC_{60}BM$-G2 (inverted PSCs, W/ $PC_{60}BM$-G2, ITO/ZnO/$PC_{60}BM$-G2/PBDT-DTBT:$PC_{71}BM$/MoO_3/Ag), and inverted PSCs without $PC_{60}BM$-G2 (inverted PSCs, W/O $PC_{60}BM$-G2, ITO/ZnO/PBDT-DTBT/$PC_{71}BM$/MoO_3/Ag) (a) in the dark and (b) under illumination.

inverted PSCs with and without the $PC_{60}BM$-G2 interfacial layer in the dark and under illumination of white light with the light intensity of 100 mW/cm^2. It is found that the dark current densities under reverse bias from the inverted PSCs with the $PC_{60}BM$-G2 interfacial layer are more than 100 times less than those from the inverted PSCs without the $PC_{60}BM$-G2 interfacial layer. These low dark current densities indicate that the bimolecular charge recombination is probably suppressed by the $PC_{60}BM$-G2 interfacial layer.[23] Thus, both higher J_{SC} and higher FF are expected to be observed from the inverted PSCs with the $PC_{60}BM$-G2 interfacial layer rather than in the inverted PSCs without the $PC_{60}BM$-G2 layer.[24−28]

Under illumination, the conventional PSCs show a J_{SC} of 11.3 mA/cm^2, a V_{OC} of 0.78 V, an FF of 62.4%, and a corresponding PCE of 5.50%. The inverted PSCs without the $PC_{60}BM$-G2 interfacial layer exhibit a J_{SC} of 11.1 mA/cm^2, a V_{OC} of 0.74 V, an FF of 58.1%, and a corresponding PCE of 4.77%. After using a thin neutral $PC_{60}BM$-G2 layer to reengineer the surface of the ZnO EEL, the inverted PSCs show a J_{SC} of 14.0 mA/cm^2, a V_{OC} of 0.73 V, an FF of 62.8%, and a corresponding PCE of 6.42%. The larger J_{SC} observed from the inverted PSCs with the $PC_{60}BM$-G2 interfacial layer is in agreement with the expectation obtained from dark $J-V$ curves, as shown in Figure 2a. Overall, there is over a 30% enhancement for PCE from the inverted PSCs with the $PC_{60}BM$-G2 layer as compared to those without the $PC_{60}BM$-G2 layer. The enhanced PCE from the inverted PSCs with the $PC_{60}BM$-G2 layer as compared with the normal device suggests that the inverted device could perform better than the normal device. More than 200 devices for each type of PSC were fabricated and characterized under the same conditions. The deviation in PCEs is less than 5%.

Approximately the same V_{OC} observed from the inverted PSCs with and without the $PC_{60}BM$-G2 indicates that there is no dipole moment formed at the interface between the EEL and BHJ composite.[6−8,15] In order to further verify it, the role of the thin film of $PC_{60}BM$-G2 used as a cathode interfacial buffer layer in the conventional PSCs was also investigated. The details of device fabrication and characterization of the conventional PSCs with a structure of ITO/MoO_3/BHJ composite/$PC_{60}BM$-G2/Al are provided in the Supporting Information. The performance parameters of the conventional PSCs are summarized in Table S1 (Supporting Information). It was found that there is no enlarged V_{OC} observed from the conventional PSCs incorporated with $PC_{60}BM$-G2, but there was more than a 20% enhancement of PCE, in particular in J_{SC} (Supporting Information, Figure S6). These results further indicate that there is no dipole moment induced by the thin layer of $PC_{60}BM$-G2, but an enhancement in J_{SC} of the conventional PSCs is due to interfacial reengineering of the BHJ composite.

In $PC_{60}BM$-G2, the N atom exists in amide, not in the amine group. The N atom in $PC_{60}BM$-G2 cannot be ionized in either methanol or water solvent. Therefore, no dipole moment is introduced on either the surface of the ZnO EEL or the BHJ active layer after depositing $PC_{60}BM$-G2 on top of the ZnO EEL and BHJ active layer.[15] In both conventional and inverted PSCs incorporated with $PC_{60}BM$-G2, no dipole moment that originated from $PC_{60}BM$-G2 was involved in the enhanced PCE. To understand the underlying physics of the enhanced PCE of the inverted PSCs, both series resistance (R_S) and sheet resistance (R_{SH}) are estimated from $J-V$ curves. The estimated R_S and R_{SH} are summarized in Table 1. With incorporation of $PC_{60}BM$-G2 on the ZnO EEL, the R_S decreased from 12.2 to 7.5 Ω cm^2. The R_{SH} in the inverted PSCs with the $PC_{60}BM$-G2 interfacial layer is 907 Ω cm^2, which is larger than that without

Table 1. Summary of Device Performance

device structure[a]	V_{OC} (V)	J_{SC} (mA/cm^2)	FF (%)	PCE (%)	R_s (Ω cm^2)	R_{SH} (Ω cm^2)
ITO/ZnO/BHJ composite/MoO_3/Ag	0.74(0.74)[b]	11.1(11.7)	58.1(60.2)	4.77(4.90)	12.2	805
ITO/ZnO/$PC_{60}BM$-G2/BHJ composite/MoO_3/Ag	0.73(0.73)	14.0(15.1)	62.8(64.0)	6.42(6.71)	7.5	907
ITO/PEDOT:PSS/BHJ composite/Al	0.78	11.3	62.4	5.5		

[a]BHJ composite: PBDT-DTBT:$PC_{71}BM$. [b]Data in ( ) represent the best device performance parameters.

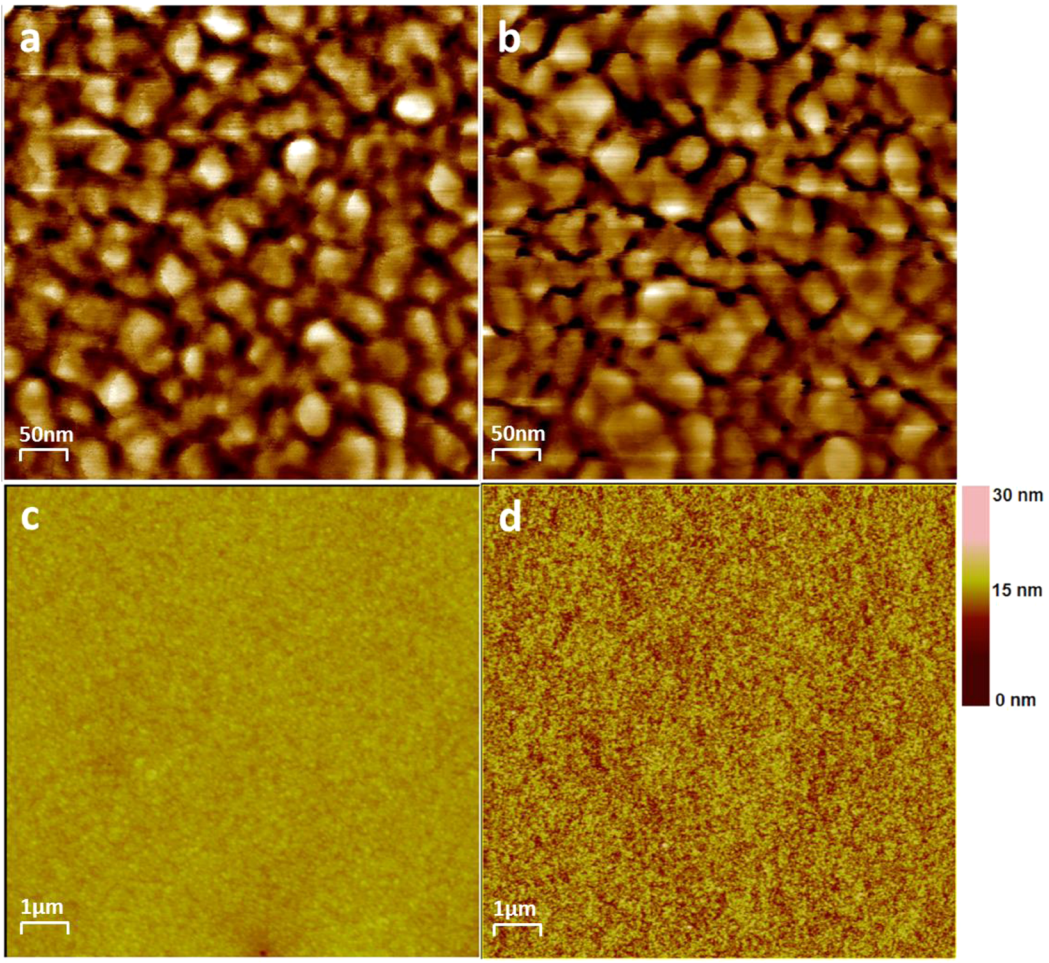

Figure 3. AFM phase images of BHJ active layer on 500 nm × 500 nm (a) pristine ZnO, and (b) $PC_{60}BM$-G2/ZnO; and AFM height images of (c) pristine ZnO, and (d) $PC_{60}BM$-G2/ZnO on 10 μm × 10 μm.

the $PC_{60}BM$-G2 interfacial layer, 805 Ω cm^2. Generally, enhanced device performance can be expected with larger R_{SH} and smaller R_S.[29,30] Therefore, the inverted PSCs with the $PC_{60}BM$-G2 interfacial layer possesses high PCE.

In order to further study the underlying device performance, atomic force microscopy (AFM) was carried out to investigate the thin film morphology of the PBDT-DTBT:$PC_{71}BM$ BHJ composite on top of pristine ZnO and $PC_{60}BM$-G2/ZnO. Figure 3a shows the phase image of the BHJ composite on pristine ZnO. The domain size of $PC_{71}BM$ aggregation is 34 ± 3 nm, and the domain size of PBDT-DTBT is 15 ± 6 nm. Figure 3b shows the phase image of the BHJ composite on $PC_{60}BM$-G2/ZnO. The domain size of $PC_{71}BM$ aggregation is 32 ± 5 nm, and the domain size of PBDT-DTBT is 13 ± 8 nm. The BHJ composite spin-coated either on ZnO or on $PC_{60}BM$-G2/ZnO exhibits appropriate phase separation and domain size for charge separation.[2] The domain size of each component in the BHJ composite has little variation when the BHJ composite is spin-coated on ZnO or $PC_{60}BM$-G2/ZnO layers. These results indicate that charge dissociation and charge transport in the BHJ composite could be similar in the devices with and without the $PC_{60}BM$-G2 interfacial layer. Therefore, with the same light absorption and charge dissociation in both devices, the enhanced PCE by the thin layer of $PC_{60}BM$-G2 solely resulted from the $PC_{60}BM$-G2/ZnO EEL.

The AFM height images of the $PC_{60}BM$-G2/ZnO and pristine ZnO EEL are shown in Figure 3c,d. The root-mean-square roughness (RMS) of $PC_{60}BM$-G2/ZnO is 1.605 nm, which is higher than that of the pristine ZnO thin film (1.320 nm). The rougher surface could provide a larger surface area and, hence, larger interfacial adhesion between the $PC_{60}BM$-G2/ZnO EEL and the BHJ active layer.[31,32] Moreover, high interfacial interactions between the $PC_{60}BM$-G2/ZnO EEL and the BHJ active layer would facilitate the transportation of the separated electrons to the respective electrode.[32] As a result, high J_{SC} is observed from the inverted PSCs with the $PC_{60}BM$-G2/ZnO EEL.

The electronic conductivities of the pristine ZnO EEL and the thin films of $PC_{60}BM$-G2/ZnO EEL were further conducted on a Bruker Dimension Icon system with a Peak Force Tapping Tunneling AFM (PFTUNA) module.[15] Figure 4 shows the PFTUNA images of the ZnO EEL and $PC_{60}BM$-G2/ZnO EEL. The peak current observed from pristine ZnO is 2.5 pA within a 2 μm zoom, but the peak current appears only in the small domain size, not in the whole film (Figure 4a). However, under the same conditions, obvious changes were observed from the peak current image of $PC_{60}BM$-G2/ZnO. The peak current is 2.5pA, but the domain size of the peak current is significantly increased when compared to those of the pristine ZnO thin films (Figure 4b). These results indicate that the surface electronic conductivities of the $PC_{60}BM$-G2/ZnO

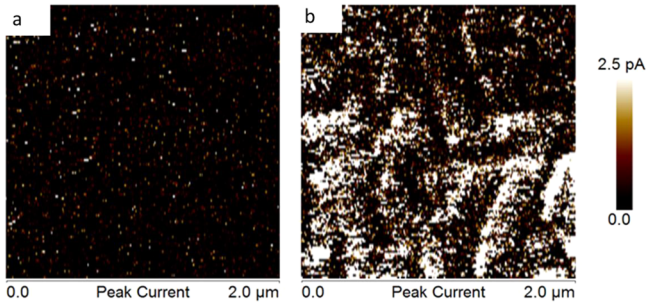

Figure 4. Peak currents on the surface of (a) ZnO and (b) $PC_{60}BM$-G2/ZnO measured by the peak force tapping tunneling AFM.

EEL are higher than those of the pristine ZnO EEL. This high surface electronic conductivity certainly facilitates the transportation of the separated electrons from the BHJ composite layer through the $PC_{60}BM$-G2/ZnO EEL to the respective cathode,[33,34] resulting in enhanced J_{SC}.

According to the band alignment shown in Scheme 2c, the hole blocking ability of $PC_{60}BM$-G2 could be another reason for enhanced J_{SC}. In order to verify it, devices with structures of ITO/ZnO/PBDT-DTBT:$PC_{71}BM$/$PC_{60}BM$-G2/MoO_3/Ag and ITO/ZnO/PBDT-DTBT:$PC_{71}BM$/MoO_3/Ag were fabricated and characterized. The $J-V$ characteristics of the above two types of PSCs are shown in Figure 5. A distinct S-shape in

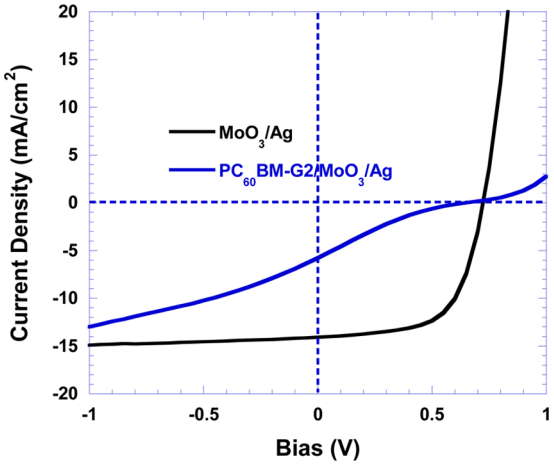

Figure 5. $J-V$ characteristics of devices ITO/ZnO/PBDT-DTBT:$PC_{71}BM$/MoO_3/Ag and ITO/ZnO/PBDT-DTBT:$PC_{71}BM$/$PC_{60}BM$-G2/MoO_3/Ag.

the $J-V$ curve of the PSCs with $PC_{60}BM$-G2 compared with that of PSCs without $PC_{60}BM$-G2 indicates that the hole transport was hindered and imbalanced hole−electron transport took place in the PSCs with $PC_{60}BM$-G2.[35] These results demonstrate that $PC_{60}BM$-G2 possess an electron-selectivity feature allowing the separated electrons and blocking the separated holes from being transported to the respective electrodes. Therefore, the recombination of electron and hole would be reduced; hence, enhanced J_{SC} and FF are expected from the PSCs incorporated with $PC_{60}BM$-G2.

CONCLUSIONS

In conclusion, a novel conductive water/alcohol-soluble neutral fullerene derivative, $PC_{60}BM$-G2, was developed and used to reengineer the surface of the ZnO electron extraction layer in the inverted PSCs. Because of the neutral property of the $PC_{60}BM$-G2, no dipole moment was introduced at the interface between the $PC_{60}BM$-G2/ZnO EEL and the BHJ composite, but an increased surface electronic conductivity of the $PC_{60}BM$-G2/ZnO EEL resulted in suppressed surface charge carrier recombination. Therefore, the same V_{OC} and dramatically increased J_{SC} and *FF*, and the consequently enhanced efficiency, were observed from the inverted PSCs with the $PC_{60}BM$-G2 interfacial layer. These results demonstrate that the surface electronic conductivity of the EEL plays an important role in the high performance of inverted PSCs.

ASSOCIATED CONTENT

Supporting Information

Additional figures and table. This material is available free of charge via the Internet at http://pubs.acs.org.

AUTHOR INFORMATION

Corresponding Author

*E-mail: xgong@uakron.edu (X.G.).

Notes

The authors declare no competing financial interest.

ACKNOWLEDGMENTS

The authors thank the Natural Science Foundation (NSF) for financial support (ECCS-1351785). The authors appreciate Dr. Steven Xiao from 1-Material Inc. for providing materials.

REFERENCES

(1) Dou, L.; You, J.; Yang, J.; Chen, C. C.; He, Y.; Murase, S.; Moriarty, T.; Emery, K.; Li, G.; Yang, Y. Tandem Polymer Solar Cells Featuring a Spectrally Matched Low-Bandgap Polymer. *Nat. Photonics* **2012**, *6*, 180−186.

(2) Gunes, S.; Neugebauer, H.; Sariciftci, N. S. Conjugated Polymer-Based Organic Solar Cells. *Chem. Rev.* **2007**, *107*, 1324−1338.

(3) Chen, L. M.; Hong, Z. R.; Li, G.; Yang, Y. Recent Progress in Polymer Solar Cells: Manipulation of Polymer:Fullerene Morphology and the Formation of Efficient Inverted Polymer Solar Cells. *Adv. Mater.* **2009**, *21*, 1434−1449.

(4) Seo, J. H.; Gutacker, A.; Sun, Y.; Wu, H.; Huang, F.; Cao, Y.; Scherf, U.; Heeger, A. J.; Bazan, G. C. Improved High-Efficiency Organic Solar Cells via Incorporation of a Conjugated Polyelectrolyte Interlayer. *J. Am. Chem. Soc.* **2011**, *133*, 8416−8419.

(5) Oh, S.-H.; Na, S.-I.; Jo, J.; Lim, B.; Vak, D.; Kim, D.-Y. Water-Soluble Polyfluorenes as an Interfacial Layer Leading to Cathode-Independent High Performance of Organic Solar Cells. *Adv. Funct. Mater.* **2010**, *20*, 1977−1983.

(6) O'Malley, K. M.; Li, C. Z.; Yip, H.-L.; Jen, A. K.-Y. Enhanced Open-Circuit Voltage in High Performance Polymer/Fullerene Bulk-Heterojunction Solar Cells by Cathode Modification with a C_{60} Surfactant. *Adv. Energy Mater.* **2012**, *2*, 82−86.

(7) Li, C. Z.; Chueh, C. C.; Yip, H. L.; O'Malley, K. N.; Chen, W. C.; Jen, A. K.-Y. Effective Interfacial Layer to Enhance Efficiency of Polymer Solar Cells via Solution-Processed Fullerene-Surfactants. *J. Mater. Chem.* **2012**, *22*, 8574−8578.

(8) Hau, S. K.; Yip, H. L.; Baek, N. S.; Zou, J.; O'Malley, K.; Jen, A. K.-Y. Air-Stable Inverted Flexible Polymer Solar Cells Using Zinc Oxide Nanoparticles as an Electron Selective Layer. *Appl. Phys. Lett.* **2008**, *92*, 253301.

(9) Luo, J.; Wu, H. B.; He, C.; Li, A. Y.; Yang, W.; Cao, Y. Enhanced Open-Circuit Voltage in Polymer Solar Cells. *Appl. Phys. Lett.* **2009**, *95*, 043301.

(10) Ma, H.; Yip, H.-L.; Huang, F.; Jen, A. K.-Y. Interface Engineering for Organic Electronics. *Adv. Funct. Mater.* **2010**, *20*, 1371−1388.

(11) Na, S.-I.; Kim, T.-S.; Oh, S.-H.; Kim, J.; Kim, S.-S.; Kim, D.-Y. Enhanced Performance of Inverted Polymer Solar Cells with Cathode Interfacial Tuning via Water-Soluble Polyfluorenes. *Appl. Phys. Lett.* **2010**, *97*, 223305.
(12) Ishii, H.; Hayashi, N.; Ito, E.; Washizu, Y.; Sugi, K.; Kimura, Y.; Niwano, M.; Ouchi, Y.; Seki, K. Kelvin Probe Study of Band Bending at Organic Semiconductor/Metal Interfaces: Examination of Fermi Level Alignment. *Phys. Status Solidi A* **2004**, *201*, 1075−1094.
(13) Zhou, H.; Zhang, Y.; Seifter, J.; Collins, S. D.; Luo, C.; Bazan, G. C.; Nguyen, T. Q.; Heeger, A. J. High-Efficiency Polymer Solar Cells Enhanced by Solvent Treatment. *Adv. Mater.* **2013**, *25*, 1646−1652.
(14) Cheng, Y. S.; Liao, S. H.; Li, Y. L.; Chen, S. A. Physically Adsorbed Fullerene Layer on Positively Charged Sites on Zinc Oxide Cathode Affords Efficiency Enhancement in Inverted Polymer Solar Cell. *ACS Appl. Mater. Interfaces* **2013**, *5*, 6665−6671.
(15) Yang, T.; Wang, M.; Duan, C.; Hu, X.; Huang, L.; Peng, J.; Huang, F.; Gong, X. Inverted Polymer Solar Cells with 8.4% Efficiency by Conjugated Polyelectrolyte. *Energy Environ. Sci.* **2012**, *5*, 8208−8214.
(16) Newkome, G. R.; Behera, R. K.; Moorefield, C. N.; Baker, G. R. Chemistry of Micelles. 18. Cascade Polymers: Syntheses and Characterization of One-Directional Arborols Based on Adamantane. *J. Org. Chem.* **1991**, *56*, 7162−7167.
(17) Cardona, C. M.; McCarley, T. D.; Kaifer, A. E. Synthesis, Electrochemistry, and Interactions with β-Cyclodextrin of Dendrimers Containing a Single Ferrocene Subunit Located "Off-Center". *J. Org. Chem.* **2000**, *65*, 1857−1864.
(18) Yang, T.; Cai, W.; Qin, D.; Wang, E.; Lan, L.; Gong, X.; Peng, J.; Cao, Y. Solution-Processed Zinc Oxide Thin Film as a Buffer Layer for Polymer Solar Cells with an Inverted Device Structure. *J. Phys. Chem. C* **2010**, *114*, 6849−6853.
(19) Sun, Q.; Wang, H.; Yang, C.; Li, Y. Synthesis and Electroluminescence of Novel Copolymers Containing Crown Ether Spacers. *J. Mater. Chem.* **2003**, *13*, 800−806.
(20) Carsten, B.; Szarko, J. M.; Son, H. J.; Wang, W.; Lu, L.; He, F.; Rolczynski, B. S.; Lou, S. J.; Chen, L.; Yu, L. Examining the Effect of the Dipole Moment on Charge Separation in DonorAcceptor Polymers for Organic Photovoltaic Applications. *J. Am. Chem. Soc.* **2011**, *133*, 20468−20475.
(21) Liao, K.-S.; Yambem, S. D.; Haldar, A.; Alley, N. J.; Curran, S. A. Designs and Architectures for the Next Generation of Organic Solar Cells. *Energies* **2010**, *3*, 1212−1250.
(22) Huang, Y.; Liu, F.; Guo, X.; Zhang, W.; Gu, Y.; Zhang, J.; Han, C. C.; Russell, T. P.; Hou, J. Manipulating Backbone Structure to Enhance Low Band Gap Polymer Photovoltaic Performance. *Adv. Energy Mater.* **2013**, *3*, 930−937.
(23) Shuttle, C. G.; O'Regan, B.; Ballantyne, A. M.; Nelson, J.; Bradley, D. D. C.; Durrant, J. R. Bimolecular Recombination Losses in Polythiophene: Fullerene Solar Cells. *Phys. Rev. B* **2008**, *78*, 113201.
(24) Cowan, S. R.; Roy, A.; Heeger, A. J. Recombination in Polymer-Fullerene Bulk Heterojunction Solar Cells. *Phys. Rev. B* **2010**, *82*, 245207.
(25) Street, R. A.; Schoendorf, M.; Roy, A.; Lee, J. H. Interface State Recombination in Organic Solar Cells. *Phys. Rev. B* **2010**, *81*, 205307.
(26) Hsieh, C. H.; Cheng, Y. J.; Li, P. J.; Chen, C. H.; Dubosc, M.; Liang, R. M.; Hsu, C. S. Highly Efficient and Stable Inverted Polymer Solar Cells Integrated with a Cross-Linked Fullerene Material as an Interlayer. *J. Am. Chem. Soc.* **2010**, *132*, 4887−4893.
(27) Cheng, Y. J.; Hsieh, C. H.; He, Y.; Hsu, C. S.; Li, Y. F. Combination of Indene-C_{60} Bis-Adduct and Cross-Linked Fullerene Interlayer Leading to Highly Efficient Inverted Polymer Solar Cells. *J. Am. Chem. Soc.* **2010**, *132*, 17381−17383.
(28) Lai, Y. Y.; Cheng, Y. J.; Hsu, C. S. Applications of Functional Fullerene Materials in Polymer Solar Cells. *Energy Environ. Sci.* **2014**, *7*, 1866−1883.
(29) Li, G.; Shrotriya, V.; Huang, J.; Yao, Y.; Moriarty, T.; Emery, K.; Yang, Y. High-Efficiency Solution Processable Polymer Photovoltaic Cells by Self-Organization of Polymer Blends. *Nat. Mater.* **2005**, *4*, 864−868.
(30) Stubhan, T.; Ameri, T.; Salinas, M.; Krantz, J.; Machui, F.; Halik, M.; Brabec, C. J. High Shunt Resistance in Polymer Solar Cells Comprising a MoO_3 Hole Extraction Layer Processed from Nanoparticle Suspension. *Appl. Phys. Lett.* **2011**, *98*, 253308.
(31) Sekine, N.; Chou, C.-H.; Kwan, W. L.; Yang, Y. ZnO Nanoridge Structure and Its Application in Inverted Polymer Solar Cell. *Org. Electron.* **2009**, *10*, 1473−1477.
(32) Ma, W.; Yang, C.; Gong, X.; Lee, K.; Heeger, A. J. Thermally Stable, Efficient Polymer Solar Cells with Nanoscale Control of the Interpenetrating Network Morphology. *Adv. Funct. Mater.* **2005**, *15*, 1617−1622.
(33) Hoppe, H.; Sariciftci, N. S. Morphology of Polymer/Fullerene Bulk Heterojunction Solar Cells. *J. Mater. Chem.* **2006**, *16*, 45−61.
(34) Yip, H. L.; Jen, A. K.-Y. Recent Advances in Solution-Processed Interfacial Materials for Efficient and Stable Polymer Solar Cells. *Energy Environ. Sci.* **2012**, *5*, 5994−6011.
(35) Tress, W.; Petrich, A.; Hummert, M.; Hein, M.; Leo, K.; Riede, M. Imbalanced Mobilities Causing S-Shaped IV Curves in Planar Heterojunction Organic Solar Cells. *Appl. Phys. Lett.* **2011**, *98*, 063301.